Finite element analysis of biomechanical variation of subchondral bone in osteoarthritis

Hainan Chen, Wei Jiang, Qirong Dong, Kan Yang

Original Article

Finite element analysis of biomechanical variation of subchondral bone in osteoarthritis

Hainan Chen[1], Wei Jiang[2], Qirong Dong[1], Kan Yang[3]

[1]Department of Orthopedics, the Second Hospital Affiliated to Soochow University, Suzhou 215004, China
[2]Department of Rehabilitation, Affiliated Hospital of Luzhou Medical College, Luzhou 646000, China
[3]Department of Orthopaedics, the Seventh People's Hospital of Suzhou, Suzhou 215004, China
Co-first author: Hainan Chen, Wei Jiang

Address correspondence to:
Qirong Dong
Department of Orthopedics,
The Second Hospital Affiliated to Soochow University,
Suzhou 215004, China
Tel: +86 512 67784116
Fax: +86 512 68284303
Email: qirongdong@163.com

ABSTRACT

Objective: This study aimed to investigate the changes of mechanical properties of subchondral bone in the early stage of knee instability and the intervention effects of diphosphate

Design: Control experiment

Setting: Second Hospital Affiliated to Soochow University, Suzhou

Subjects: Sixty healthy male New Zealand white rabbits were divided into model, diphosphate, and control groups

Intervention: Statistical analysis and comparison

Main outcome: The obtained 2D image files were then used for the finite element analysis

Results: Several parameters of the 12- and 4-week groups were compared. Results showed that bone volume fraction, bone density, elastic modulus, reaction force, and von Mises stress were all increased ($p < 0.01$). In the early stage of knee instability, the elastic modulus significantly decreased. The diphosphate could significantly improve the elastic modulus of the subchondral bone by preventing bone resorption.

Conclusions: The changes in the mechanical properties of the subchondral bone showed a significant role in the occurrence and development of osteoarthritis.

KEY WORDS: biomechanics, finite element analysis, occurrence, osteoarthritis

INTRODUCTION

Osteoarthritis (OA) is a common disease in older people[1]. It is characterized by joint pain and dysfunction[2]. However, its pathogenesis remains unclear, and many factors are involved. Biological and mechanical factors are considered to be the two major risk factors[3]. In recent years, the roles of mechanical factors in OA have received increasing attention. Moreover, several studies about the effects of cell biomechanics[4], material biomechanics[5], and subchondral bone biomechanics in OA have been conducted[6-8], and research methods have been constantly updated[9]. OA can lead to anatomical variations of subchondral trabecular bone in the femoral head and changes of trabecular 3D structure, which affect the mechanical properties of the subchondral bone[10]. By establishing a rabbit OA model, the author used micro-CT to perform the 3D reconstruction of subchondral bone. Subsequently, the finite element calculation was conducted, and the mechanical changes of the subchondral bone were observed. Meanwhile, bisphosphonate (Bis) intervention was also applied to investigate the effects of mechanical changes in the subchondral bone on OA progress.

MATERIALS AND METHODS

Experimental animals and grouping

Sixty healthy male New Zealand white rabbits (provided by the Animal Center, School of Medicine of Suzhou University) weighing 2.71 ± 0.29 kg were placed in individual cages. The rabbits were provided granulated diet and free access to drinking water. The ambient temperature was 22 ± 1 °C, with alternate natural light–dark cycles every 12 hours. The rabbits were divided into model (n = 24), Bis (n = 24), and control groups (n = 12) by using a table of random digits. This study was carried out in strict accordance with the recommendations in the Guide for the Care and Use of Laboratory Animals of the National Institutes of Health. The animal use protocol has been reviewed and approved by the Institutional Animal Care and Use Committee (IACUC) of Soochow University.

Model duplication and specimen collection

All animals underwent knee-skin preparation 1 day before the modeling and were weighed before the surgery. About 20 g/L sodium pentobarbital (Sigma Co., San Francisco, USA) was injected through an ear vein at a dose of 30 mg/kg to induce anesthesia. The animal was then disinfected and covered with an operation sheet. A medial patellar incision was made to expose the joint cavity. Joint cavity incision was conducted on the model and Bis groups. Subsequently, the anterior cruciate ligament was cut (confirmed by the drawer test). About 5 mm of the ligament was cut off from the middle segment, and the incision was sutured layer by layer. The same joint cavity incision was performed on the control group, except that the anterior cruciate ligament was only exposed instead of cut, and the incision was sutured layer by layer. The rabbits were intraperitoneally injected with cefazolin sodium (500 mg/d) (Shandong Lukang Pharmaceutical Group Co., Ltd., Shandong, Chinese) for 5 days postoperatively to prevent infection. The injured limb was not fixed, and the animals were bred separately and allowed free movement. The Bis group was subcutaneously injected daily with 0.01 mg/kg Bis (risedronate sodium; LKT Laboratories Co., Minnesota, USA), whereas the model and control groups were subcutaneously injected with equal volume of isotonic saline. The rabbits were then killed at each predetermined time point (4^{th}, 8^{th}, and 12^{th} weeks after the surgery) by air embolism. The surgical side of the knee (2 cm above and below the reserved knee plane) was cut following the removal of the soft tissues. The knee was cryopreserved at −20 °C for 48 h and then examined using micro-CT (GE Healthcare, London Ontario, Canada).

Gross scoring and Mankin scoring

Gross morphological evaluation was performed on the intra- and extra-lateral condyle cartilages of femurs. The evaluation was classified into 5 grades according to the OA standard: grade 1 (0 point), the surface was normal and smooth, without damage; grade 2 (1 point), the articular cartilage was rough, gray colored, with small cracks; grade 3 (2 points), the articular surface was erosive, with large cracks, and the cartilage defects reached the middle layer of cartilage surface; grade 4 (3 points), the ulcers and defects of articular cartilage reached the deep layer of cartilage; and grade 5 (4 points), the cartilage exfoliated, and the subchondral bone was exposed. The tissue samples were stained with hematoxylin and eosin (HE) and then observed under a microscope. Scoring was conducted referring to the Mankin scoring criteria.

Micro-CT examination and finite element analysis

The joint sample of the rabbit knee was evenly placed in the examination slot of the micro-CT system and then bundled to prevent movement. The scan was performed along the long axis of the specimen, with a scanning protocol of 45 μm, 24R, and 18 min. The scanning parameters were as follows: scan resolution, 45 μm; rotation angle, 360°; rotation angle increment, 0.5°; interlayer spacing, 20 μm; tube voltage, 80 kV; tube current, 450 μA; exposure time, 2960 ms; and scanning time, 18 min. Five hundred different sectional images (1024×1024 pixels) of the same sample were obtained, and the segmentation value was set at 1000 to complete the image binarization. The complete bone tissue of the sample was set as the region of interest (ROI) for further 3D reconstruction. 3D visualization was then performed on the selected ROI intra-bone. Micview V2.1.2 3D reconstruction processing software and ABA special bone analysis software were used for quantitative analysis.

The specific measurement parameters were as follows: bone volume fraction (BVF), namely, the division of bone volume (BV) by the total volume (TV), and expressed as %; and volumetric BMD (vBMD), namely, the apparent density of porous trabecular bone, reflecting the overall bone mineral density in the region, and expressed as mg/mm^3. 2D images in DICOM format were obtained from micro-CT and then imported into Mimics V10.01 software for fitting and threshold setting. The grid redraw module was used to generate the grid, and the Mimics main interface generated the surface mesh model, which was then transmitted into Ansys V10 for the body mesh processing. The obtained body mesh model was finally materialized in Mimics. A total of 10 types of materials were selected, with each representing the material properties of

each section. Geomagic Studio 11.0 software was used to repair and optimize the generated models. The Homminga *et al*[11] formula is as follows: $E_{element} = E_{tissued} (GV_{element})^{\gamma}$, where $E_{element}$ is the relative gray value based on each finite element ($GV_{element}$); the normal range is from 0 (bone marrow) to 1 (bone). This formula was used to converse the elastic modulus into the tissue's elasticity modulus. The normal gray value was 1754 mgHA/cm^3 (equivalent to 12000 CT). Given that the femoral condyle is composed of dense and cancellous pine mass, the dense mass is anisotropic and the cancellous mass is isotropic. Therefore, the simplified material model was unified to the isotropic linear materials. The elastic modulus ($E_{tissued}$) and index (γ) were determined based on the image resolution and structure size; according to literature, $E_{tissued}$ was set at 15 GPa, $\gamma = 1.7$[12]. The apparent elastic modulus was reversely calculated using a computer, with a Poisson's ratio of 0.3. The boundary condition was set as the stress applied, which made the femoral condyle realize 1% longitudinal compression. Thus, the reaction force and average von Mises stress, which could induce 1% deformation, were obtained.

Statistical analysis

The data were expressed as $\bar{x} \pm s$. SPSS 13.0 statistical software was used for all statistical analyses. ANOVA was performed for intergroup comparison. P-value <0.05 was considered statistically significant.

RESULTS

General observation and OA scoring of cartilages

The knee joint cavity of the control group had no joint effusion. The joint fluid was small and clear, and the joint exhibited no swelling and synovial hyperplasia. In addition, no osteophyte formation was observed. The articular cartilages of the femoral condyle and tibial plateau were blue and white, and bright and smooth, respectively. At the 4th week, joint effusion and synovial hyperplasia appeared in 2 cases of the model group, and the articular surface was erosive and rough. At the 12th week, the synovium exhibited nodular hyperplasia, and the synovial fluid was cloudy. The surface of the two femoral articular condyle exhibited large cracks and ulcers. The cartilage damages of the Bis group were significantly reduced than those of the model group at the 4th and 12th weeks, as shown in Table 1.

Mankin scoring of articular cartilage injury

The tissue samples were stained with HE and then observed under a microscope. Scoring was performed referring to the Mankin scoring criteria, as shown in Table 2. The control side exhibited normal articular cartilage at the 4^{th} and 12^{th} weeks, and the Mankin scores were 0-1 point. HE staining showed that the chondrocytes were uniformly distributed, with clear layers and neat arrangements. The tidal line was intact. Moreover, the toluidine blue staining was uniform, and no staining loss was observed. At the 4^{th} week, the model group exhibited a nonflat cartilage surface. The chondrocytes showed compensatory proliferation and were disorganized; some even appeared in clusters. The chondrocytes with larger volume exhibited a tendency to migrate toward the cartilage surface. Mild loss of toluidine blue staining was observed. At the 12^{th} week, the damages of the articular cartilage were severe, and the tidal line disappeared. Pathological changes, such as disappearance of cartilage and exposure of subchondral bone, were found. Osteophyte formation also occurred. The toluidine blue staining disappeared. Compared with the Bis and control groups, the model group showed cartilage degeneration ($p < 0.01$), which further aggravated at the 12^{th} week ($p < 0.01$). The degeneration at the 12^{th} week was significantly worse than that at the 4^{th} week, ($p < 0.01$). The Bis group exhibited less degeneration than the model group at the 4^{th} and 12^{th} weeks ($p < 0.01$) and showed no statistical significance with the control group.

Structures and mechanical parameters

The BVF, Tb.Th, Tb.N, Tb.Sp, and bone density of the 60 specimens were obtained through micro-CT examination. The finite element software was used to calculate the elastic modulus (EM), reaction force (RF), and average von Mises stress. At postoperative 4^{th} week, the BVF, EM, RF, and average von Mises stress of the model group were decreased when compared with those of the Bis and control groups; the model group was significantly lower than the Bis and control groups ($p < 0.01$). These parameters were also decreased in the Bis group when compared with those of the control group, but the difference was not statistically significant. The bone density of the model group was significantly lower than that of the control and Bis groups ($p < 0.01$). However, the comparison between the Bis and control groups exhibited no statistically significant difference (Table 3). At the 12^{th} week, the BVF and BMD of the model group was significantly increased than those of the control and Bis groups ($p < 0.01$), whereas the Em, RF, and von Mises stress were decreased ($p < 0.05$) (Table 4). The Bis group was also lower than the

control group, but the difference was not statistically significant. The BVF, BMD, EM, RF, and von Mises stress at the 12th week were increased when compared with those at the 4th week ($p < 0.01$) (Table 5). Meanwhile, the 2D DICOM images and 3D reconstruction images exhibited that the osteophytes of the model group were significantly proliferated than those of the Bis and control groups (Figure 1). A: 2D DICOM and 3D reconstruction images of knee joint of the control group. A1: 2D DICOM; A2: Normal position; A3: Right side; B: 2D DICOM and 3D reconstruction images of knee joint of the model group; B1: Osteophyte in 2D DICOM; B2: Osteophyte in normal position; B3: Osteophyte exhibited in lateral position; C: 2D DICOM and 3D reconstruction images of knee joint of the Bis group; C1: Osteophyte in 2D DICOM; C2: Osteophyte in normal position; C3: Osteophyte in lateral position.

Correlation comparison

At postoperative 4th week, the EM of the model group was negatively correlated with Mankin scores ($r = -0.835$, $p < 0.01$), but positively correlated with BMD ($r = 0.848$, $p < 0.01$) and volume fraction ($r = 0.893$, $p < 0.01$). At postoperative 12th week, the EM of the model group was negatively correlated with Mankin scores ($r = -0.883$, $p < 0.01$), but positively correlated with BMD ($r = 0.861$, $p < 0.01$) and volume fraction ($r = 0.817$, $p < 0.01$).

DISCUSSION

Because of its special structure, the subchondral bone, has special functions in joint movements. This bone absorbs the stress placed on the articular surface and then distributes it to the backbone and its surrounding tissues, thus buffering the shocks from the joints and protecting the articular cartilage and other vital organs. Meanwhile, the subchondral bone maintains the unique shapes of different joints, making it easier to perform their functions. All these functions require the subchondral bone to have sufficient strength (*i.e.*, the ability to resist the damages when bearing the loadings) and stiffness (*i.e.*, the ability to resist the deformation under the extra loadings)[13].

Numerous measurement methods and mechanical property studies of knee subchondral bone are available. A bone density detection instrument was commonly used to detect subchondral bone density. Through this evaluation, the relationships between the subchondral bone density and articular cartilage damage were investigated. Mckinley *et al*[14] used high-resolution digital imaging and built-in software to measure the sclerotic model of

subchondral bone of human cadavers. They found that the stress on the peri-joint trabecular bone is increased because of the sclerosis of the subchondral bone, exhibiting weakened cushioning and protective effects on the articular cartilage. This phenomenon indirectly results in cartilage destruction. A hydraulic mechanical material testing machine was used to prepare a special stainless steel cylindrical indenter and load the oppression on the experimental zone of subchondral bone of the rabbit tibial plateau. The results indicated that the stiffness and strength of rabbit knee in the entire procedure changed from low to high in the early stage of instability. Meanwhile, he studied the correlations between the EM changes and articular cartilage damages. With the development and application of non-invasive and higher resolution equipment, such as CT and MRI, as well as the continuous innovation of computer software, the 3D finite element method is widely applied in biomechanical studies. Previously, this method was used in spine research and then gradually applied to mechanical studies of the skull, pelvis, and limb joints. The development of micro-CT, which is suitable for small animal studies, such as bone anatomy, including teeth, and bone specimens, as well as the limb bones of live animals, greatly contributes to research about bone structures and mechanical properties for clinical and basic needs[15-17].

In this experiment, an unstable model of the rabbit knee was first established. The femoral distal articular bone was then intercepted, and micro-CT scanning was conducted. Mimics software fitting was used for the images obtained to initially form the 3D model, which was then imported into the Geomagic software for refinement and formation of the 3D solid model that could be recognized by the finite element analysis software. This 3D solid model of bone tissues was then calculated using Ansys software. Subsequently, reverse engineering was performed to calculate the relevant data. Through fixing the nodes, the restraints were loaded to observe the experimental indicators. The results indicated that in the early stage of knee instability (4 weeks after the surgery), the comparison between the model and Bis groups revealed that BVF and BMD, which could reflect the bone mass, were significantly reduced ($p < 0.01$). The EM, RF, and von Mises stress were also significantly reduced; the Bis group was also lower than the control group, but the difference was not significant. This result indicates that in the early OA stage, the knee was unstable because the cruciate ligament was cut off. Thus, the joint was affected by abnormal forces. Moreover, the subchondral bone exhibited structural changes, and the bone mass was reduced. The EM, RF, and von Mises stress, which could reflect the mechanical strength of subchondral bone, were slightly reduced. At 12 weeks after the surgery, although the

BVF, BMD, EM, RF, and von Mises stress were still lower than those of the control group ($p < 0.05$), they were significantly improved than those at postoperative 4th week. The bone density of certain specimens was even higher than that of the control group. This finding reveals that the structure and mechanical strength of subchondral bone in the entire process changed from low to high in the early OA stage, namely, the compliance was initially increased then decreased; these results are similar to those reported in literature[15]. Meanwhile, the early EM value of the OA model was related to the articular cartilage scoring, BVF of subchondral bone, and bone density. EM was negatively correlated with Mankin scores at the 4th week, but positively correlated with BVF and BMD of subchondral bone. At the 12th week, EM was negatively correlated with Mankin scores, but positively correlated with BVF and BMD of subchondral bone. This demonstrates the relationship of mechanical properties and structures of subchondral bone in the early OA stage, *i.e.*, more bone mass indicates better bone structure and mechanical properties, and reflects the changes in OA.

The exact mechanism of mechanical property changes of subchondral bone is not completely elucidated. Fazzalari *et al*[17-20] believed that abnormal stress causes subchondral bone micro-fractures. These micro-fractures result in bone remodeling, as well as simultaneous activation of osteoblasts and osteoclasts and secretion of various proteases and cytokines, which lead to subchondral bone resorption, bone mass destruction, and trabecular bone fracture. Thus, abnormal stress inevitably causes the reduction of mechanical properties. Meanwhile, bone repair begins, but the destruction and repair are uneven. Calcium deposition is not sufficient, thus decreasing bone density. With the development of disease, repair and calcium deposition are increased, resulting in accelerated subchondral bone remodeling and evident reconstruction, which leads to bone sclerosis. At this time, the EM, bone density, and stress intensity are increased. However, because of excessive subchondral bone sclerosis, its capacity of buffering the joint also drops, so that its stress reverse reaction on the articular cartilage increases, which further promotes articular cartilage destruction. In this study, the general observations were consistent with the aforementioned findings. Regarding the sequence of these changes, namely, whether the cartilage changes first, then affects the subchondral bone, or the subchondral bone changes first, then affects the cartilage, or these two change at the same time, remains unclear[21-23]. However, studies reported that the changes of subchondral bone are observed prior to the cartilage in OA animal models of primates and the spontaneous OA model of guinea pigs[24].

In this study, it was also observed that the structural characteristics and mechanical indexes of subchondral bone in the bisphosphonates group were significantly higher than those in the model group, indicating that bisphosphonates can significantly protect the structure and mechanical properties of subchondral bone. As the third generation of bisphosphonates, sodium rizonium is a synthetic pyrophosphate analogue. The difference in the chemical structure between bisphosphonates and pyrophosphate lies in the substitution of P - O - P bond for P - C - P bond. This substitution makes it resistant to the action of the hydrolase without biodegradation, and its hydroxyl group and 2 phosphate groups make it highly compatible to the bone matrix. The author believed that osteoclasts are target cells of bisphosphonates, which can significantly inhibit the bone resorption of osteoclasts, promote the apoptosis of osteoclasts and inhibit the formation of osteoclasts. Our results also showed that bisphosphonates can effectively inhibit bone destruction, protect the mechanical properties of subchondral bone, reduce bone remodeling and protect articular cartilage. Our previous study[25] showed that the volume fraction (BVF) of bone trabecula, bone trabecular number (Tb.N) and bone trabecular thickness (Tb.Th) of the subchondral bone in rabbit gonarthrosis model at postoperative 4 weeks were significantly reduced as compared with those of the control group, while the bone trabecular separation (Tb.Sp) was increased and the bone mineral density (vBMD) decreased, which indicated that there is abnormal force on articular surface caused by various pathogenic factors in early stage of osteoarthritis. The bone trabecula of subchondral bone is damaged by repeated overload pressure, and then causes edema, hemorrhage and necrosis of bone marrow locally. The repeated microdamage of the subchondral bone and calcified cartilage initiate the process of bone remodeling, activate osteoclast, decompose a variety of osseous enzymes, promote local osteolysis and destroy the structure of the trabecular bone. At the same time, the neovascularization and the activated osteoblasts promote the formation of new bone and the production of osteoid, but the calcification is not enough, presenting as the decrease of the volume fraction, trabecular bone volume, thickness and bone mineral density. Because the bone density of the subchondral bone is reduced and the structure is destroyed, the mechanical properties will inevitably decrease. The buffer capacity of subchondral bone is not enough for the force from the cartilage, so that the articular cartilage cannot be well protected. The microstructural parameters of the bisphosphonates group were statistically different from that of the model group, indicating the protective effect of bisphosphonates on the destruction of subchondral bone tissue. Meanwhile, we compared bone mineral density and bone trabecular

structure between 4 and 12 weeks, and found that BVF, Tb.N, TbTh and vBMD were increased significantly at 12 weeks ($p < 0.05$), while the bone trabecular space was decreased ($p < 0.01$). There was no significant difference between the bisphosphonates group and the control group, suggesting an obvious bone destruction in early OA and an accelerated bone formation in the later stage. Early OA showed accelerated bone remodeling with insufficient calcification, destroyed bone trabecular structure and reduced mechanical properties. However, with the repair and reconstruction of subchondral bone in the later stage, the subchondral bone was hardened, resulting in increased hardness of subchondral bone. The uneven hardness of the subchondral bone changed the stress balance of articular cartilage and aggravated the cartilage damage. However, there was a significant difference in various parameters between the bisphosphonates group and the model group, indicating that bisphosphonates could protect the subchondral bone tissue which had been damaged. The general observation of the articular cartilage of the bisphosphonates group in the same period was obviously better than that of the model group, also proving that bisphosphonates can be used as a potential therapeutic drug for osteoarthritis. The mechanism of sodium rizonium protecting the subchondral bone may be that bisphosphonates can inhibit the enzymolystic effect of a variety of matrix metalloproteinase (MMPs), cathepsin K and other proteases produced by osteoclasts on the subchondral bone. In addition, bisphosphonates can promote the apoptosis of macrophages, inhibit the bone remodeling of subchondral bone, reduce the destruction of subchondral bone, and thereby reducing the occurrence of subchondral osteosclerosis.

The accuracy of the finite element analysis mainly depends on two aspects: the coincidence degree of model and actual tissue and the choice of loading constraints. In the present study, high-resolution micro-CT was used to examine the rabbit knee joint. This technique could reflect the trabecular bone structure from the microstructural aspect. The loading conditions should be in line with the actual situation as much as possible. Although the muscles around the joint are neglected in the finite element analysis, and the complexity of the actual joint movement is not completely considered, this method possesses evident advantages. It can overcome the effects of conventional experiment objects, design methods, and other factors on the results, as well as exclude errors due to different experimental conditions. In this method, one or several parameters can be changed to observe their effects on the entire system. In addition, calculation can be repeated, which is cost-efficient. In this study, the parameters were designed according to the reported standard[26]. This could ensure the accuracy and versatility of the model,

establishing a good foundation for further studies.

CONCLUSION

The changes in the mechanical properties of the subchondral bone showed a significant role in the occurrence and development of osteoarthritis.

ACKNOWLEDGMENT

Conflict of interest: All authors have no conflict of interest regarding this paper.

REFERENCES

1. Yohannes AM, Caton S. Management of depression in older people with osteoarthritis: A systematic review. Aging Ment Health 2010; 14:637-651.
2. Wu YS, Hu YY, Yang RF, Wang Z, Wei YY. The matrix metalloproteinases as pharmacological target in osteoarthritis: statins may be of therapeutic benefit. Med Hypotheses 2007; 69:557-559.
3. Atik OS, Erdogan D, Seymen CM, Bozkurt HH, Kaplanoglu GT. Is there crosstalk between subchondral bone, cartilage, and meniscus in the pathogenesis of osteoarthritis? Eklem Hastalik Cerrahisi 2016; 27:62-67.
4. Issa RI, Griffin TM. Pathobiology of obesity and osteoarthritis: integrating biomechanics and inflammation. Pathobiol Aging Age Relat Dis 2012; 2.
5. Bailey AJ, Mansell JP, Sims TJ, Banse X. Biochemical and mechanical properties of subchondral bone in osteoarthritis. Biorheology 2004; 41:349-358.
6. Day JS, Van Der Linden JC, Bank RA, *et al*. Adaptation of subchondral bone in osteoarthritis. Biorheology 2004; 41:359-368.
7. Li G, Yin J, Gao J, *et al*. Subchondral bone in osteoarthritis: insight into risk factors and microstructural changes. Arthritis Res Ther 2013; 15:223.
8. Zhen G, Wen C, Jia X, *et al*. Inhibition of TGF-beta signaling in mesenchymal stem cells of subchondral bone attenuates osteoarthritis. Nat Med 2013; 19:704-712.
9. Tsouknidas A, Anagnostidis K, Panagiotidou S, Michailidis N. The effect of osteoarthritis on the regional anatomical variation of subchondral trabecular bone in the femoral head. Clin Biomech (Bristol, Avon) 2015; 30:418-423.
10. Chen H, Dong Q, Jiang W. 3-D Structural Changes in Subchondral Bone and the Effect of

Bisphosphonate Intervention in Early Osteoarthritis. Inter J Morpho 2016; 34:291-297.

11. Homminga J, Huiskes R, Van Rietbergen B, Ruegsegger P, Weinans H. Introduction and evaluation of a gray-value voxel conversion technique. J Biomech 2001; 34:513-517.
12. Macneil JA, Boyd SK. Bone strength at the distal radius can be estimated from high-resolution peripheral quantitative computed tomography and the finite element method. Bone 2008; 42:1203-1213.
13. Teo JC, Si-Hoe KM, Keh JE, Teoh SH. Relationship between CT intensity, micro-architecture and mechanical properties of porcine vertebral cancellous bone. Clin Biomech (Bristol, Avon) 2006; 21:235-244.
14. McKinley TO, Borrelli J Jr, D'Lima DD, Furman BD, Giannoudis PV. Basic science of intra-articular fractures and posttraumatic osteoarthritis. J Orthop Trauma 2010; 24:567-570.
15. Mohan G, Perilli E, Parkinson IH, Humphries JM, Fazzalari NL, Kuliwaba JS. Pre-emptive, early, and delayed alendronate treatment in a rat model of knee osteoarthritis: effect on subchondral trabecular bone microarchitecture and cartilage degradation of the tibia, bone/cartilage turnover, and joint discomfort. Osteoarthritis Cartilage 2013; 21:1595-1604.
16. Xia Z, Zhou C, Yong Q, Wang X. On selection of repeated unit cell model and application of unified periodic boundary conditions in micro-mechanical analysis of composites. Int Solids Struc 2006; 43:266-278.
17. Li ZC, Dai LY, Jiang LS, Qiu S. Difference in subchondral cancellous bone between postmenopausal women with hip osteoarthritis and osteoporotic fracture: implication for fatigue microdamage, bone microarchitecture, and biomechanical properties. Arthritis Rheum 2012; 64:3955-3962.
18. Chiba K, Osaki M, Ito M, Majumdar S. Osteoarthritis and bone structural changes. Clin Calcium 2013; 23:973-981.
19. Kraus VB, Feng S, Wang S, *et al*. Subchondral bone trabecular integrity predicts and changes concurrently with radiographic and magnetic resonance imaging-determined knee osteoarthritis progression. Arthritis Rheum 2013; 65:1812-1821.
20. Ratzlaff C, Guermazi A, Collins J, *et al*. A rapid, novel method of volumetric assessment of MRI-detected subchondral bone marrow lesions in knee osteoarthritis. Osteoarthritis Cartilage 2013; 21:806-814.
21. Kwon OR, Kang KT, Son J, *et al*. Biomechanical comparison of fixed- and mobile-bearing for

unicomparmental knee arthroplasty using finite element analysis. J Orthop Res 2014; 32:338-345.

22. Della Croce U, Crapanzano F, Li L, *et al*. A preliminary assessment of a novel pneumatic unloading knee brace on the gait mechanics of patients with knee osteoarthritis. PM R 2013; 5:816-824.
23. Cox LG, van Donkelaar CC, van Rietbergen B, Emans PJ, Ito K. Alterations to the subchondral bone architecture during osteoarthritis: bone adaptation vs endochondral bone formation. Osteoarthritis Cartilage 2013; 21:331-338.
24. McErlain DD, Milner JS, Ivanov TG, Jencikova-Celerin L, Pollmann SI, Holdsworth DW. Subchondral cysts create increased intra-osseous stress in early knee OA: A finite element analysis using simulated lesions. Bone 2011; 48:639-646.
25. Chen H, Dong Q, Jiang W. 3-D Structural changes in subchondral bone and the effect of bisphosphonate intervention in early osteoarthritis. Int J Morphol 2016; 34:291-297.
26. Tsouknidas A, Savvakis S, Asaniotis Y, Anagnostidis K, Lontos A, Michailidis N. The effect of kyphoplasty parameters on the dynamic load transfer within the lumbar spine considering the response of a bio-realistic spine segment. Clin Biomech (Bristol, Avon) 2013; 28:949-955.

Table 1: OA scores of the 3 groups ($\bar{x}$ ±s)

Group	Number	Postoperative 4th week	Postoperative 12th week
Model	12	0.88 ± 0.6409[a]	3.25 ± 0.7071[ad]
Bis	12	0.38 ± 0.5176[b]	1.63 ± 0.7440[c]
Control	6	0.13 ± 0.3536	0.38 ± 0.5176

Compared with the control group, [a] p <0.01; compared with the model group, [b] p <0.05, [c] p <0.01; compared with the 4th week, [d] p <0.01

Table 2: Mainkin scores of the 3 groups ($\bar{x}$ ±s)

Group	Rabbits	Postoperative 4th week	Postoperative 12th week
Model	12	4.53±0.1444[a]	8.56±1.6832[ad]
Bis	12	1.98±0.1931[b]	2.50±0.1581[c]
Control	6	1.41±0.0207	1.40±0.1681

Compared with the control group, [a] p <0.01; compared with the model group, [b] p <0.05, [c] p <0.01; compared with the 4th week, [d] p <0.01

Table 3: Comparison of distal femoral microstructures and mechanical parameters of the 3 groups on the postoperative 4th week ($\bar{x}$ ±s)

Group	Animal number	The postoperative 4th week				
		BVF(%)	vBMD(mg/mm^3)	EM(MPa)	RF(N)	VM(MPa)
Model	12	26.44±1.81	298.66±4.68	175.46±1.55	368.41±1.72	9.41±1.62
Bis	12	30.03±2.42	305.38±2.40	227.96±1.87	383.52±1.54	16.42±1.63
Control	6	34.10±1.78	308.52±2.21	230.54±1.73	390.90±7.74	18.33±1.59
p		[a](p<0.05)	[a](p<0.05)	[a](p<0.01)	[a](p<0.01)	[a](p<0.01)
		[b](p<0.01)	[b](p<0.01)	[b](p<0.01)	[b](p<0.01)	[b](p<0.01)
		[c](p<0.05)				

Note: Among the P values, a: comparison between the model group and the bis group; b: comparison between the model group and the control group; c: comparison between the bis group and the control group.

Table 4: Comparison of distal femoral microstructures and mechanical parameters of the 3 groups on the postoperative 12th week ($\bar{x}$ ±s)

Group	Animal number	The postoperative 12th week				
		BVF(%)	vBMD(mg/mm^3)	EM(MPa)	RF(N)	VM(MPa)
Model	12	41.21±2.21	319.59±4.08	270.32±1.65	374.25±1.68	11.55±1.18
Bis	12	36.13±2.16	310.71±1.80	227.36±1.60	382.34±6.83	16.44±1.43
Control	6	35.00±2.86	308.57±2.91	229.48±1.85	388.49±1.55	18.43±1.39
P		[a](p<0.01)	[a](p<0.01)	[a](p<0.01)	[a](p<0.05)	[a](p<0.01)
		[b](p<0.01)	[b](p<0.01)	[b](p<0.01)	[b](p<0.01)	[b](p<0.01)

Note:Among the P values a: comparison between the model group and the bis group; b: comparison between the model group and the control group.

Table 5: Comparison of distal femoral microstructures and mechanical parameters of the model group between the postoperative 4th and 12th week ($\bar{x}$ ±s)

Group	Animal number	The postoperative 12th week				
		BVF(%)	vBMD(mg/mm^3)	EM(MPa)	RF(N)	VM(MPa)
The postoperative 4th week	12	26.44±1.81	298.66±4.68	175.46±1.55	368.41±1.72	9.41±1.62
The postoperative 12th week	12	41.21±2.21	319.59±4.08	270.32±1.65	374.25±1.68	11.55±1.18
p		<0.01	<0.01	<0.01	<0.01	<0.05

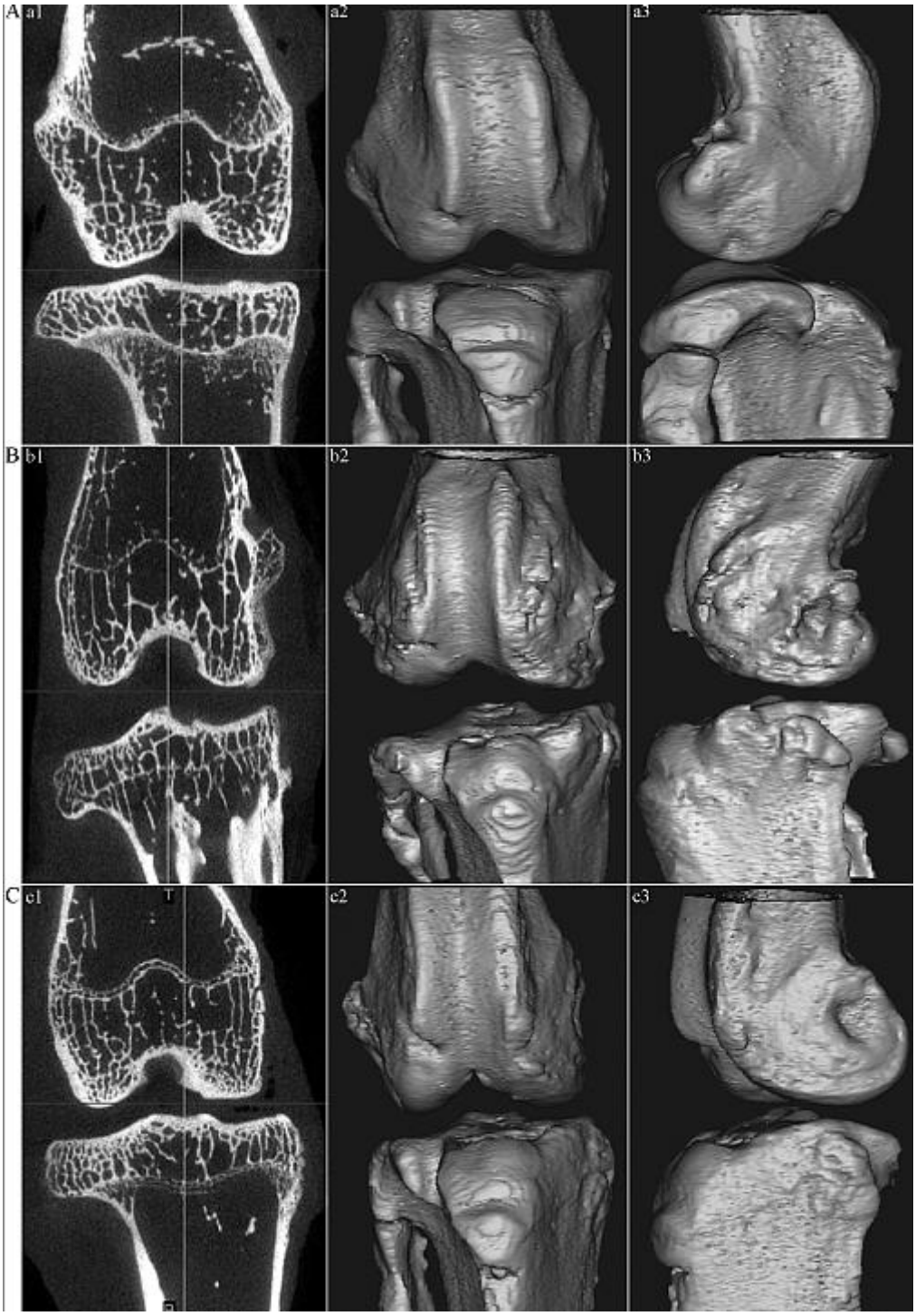

Figure 1: 3D reconstruction figures of knee at different times.
A. 2D DICOM and 3D reconstruction of knee joint in the control group;
B. 2D DICOM and 3D reconstruction of knee joint in the model group;
C. 2D DICOM and 3D reconstruction of knee joint in the diphosphate group